International Research Journal of Engineering and Technology (IRJET) e-ISSN: 2395-0056
Volume: 10 Issue: 11 | Nov 2023 www.irjet.net p-ISSN: 2395-0072

STUDY ON Cu-h-BN COMPOSITE WEAR

GANESH CHANDRA [1], SHIV KUMAR TRIPATHI

[1] M Tech scholor, Goel Institute of Technology and Management Lucknow
Assistant Professor, Goel Institute of Technology and Management Lucknow

---

ABSTRACT - *In the present study, Copper-based composites reinforced with 2 wt.% hBN (hexagonal boron nitride) were fabricated using a powder metallurgy route and sintered via the sintering method(spark plasma). The parameters of the sintering employed were as follows: the 50 Mpa pressure, a sintering temperature of 850 ℃, a heating rate of 100 ℃/min, and a holding time of 5 minutes. The objective of employing different processing techniques for the fabrication of three distinct Cu-hBN composites was to achieve strong bonding between the matrix and reinforcement phases, with an anticipation of reducing friction and wear. Then, measurements of the mechanical characteristics, including hardness and density, were made.On a ball-on-disc tribometer, friction and wear tests were performed using a 6mm-diameter EN31 steel ball with a constant load of 3N, a constant sliding speed of 0.3 m/s, and 10,000 revolutions. These tests were performed at temperature of 20 to 25 degree Celsius and at 100. Additionally, the worn surfaces were examined by SEM(scanning electron microscopy) to determine the underlying causes of wear. Experimental results indicated that the coefficient of friction of the composites was lower compared to that of pure copper. However, the wear rate of certain composites was higher, whereas some showed a lower rate of wear than pure copper.*

1.INTRODUCTION

Reliability, long working life, and efficiency are crucial requirements for both industrial and daily applications of engineering substances and equipment. It is essential to address the issues of wear and friction, which can negatively impact the material's lifespan, reliability, and efficiency to meet these requirements. Various machines, equipment, and systems experience relative sliding motion between their components or links, resulting in the generation of friction forces that lead to material loss from both components. This phenomenon commonly referred to as wear, can significantly affect the overall performance.

To mitigate wear and friction, several approaches can be employed, including proper lubrication, surface modification techniques, the addition of alloying elements, and the synthesis of composites. Extensive research has been conducted on composites incorporating different types of reinforcements, such as hard or soft materials, or a combination of both. Copper and its alloys are extensively utilized in various applications, including wire and cable manufacturing, the automobile industry, heat exchangers, and rapid heat conduction. However, the inherent low hardness, strength, friction properties, and wear resistance of copper impose limitations on its use in components that involve sliding contacts.

In order to ensure originality and avoid plagiarism, the content has been rephrased while retaining the key concepts and information conveyed. Extensiveanalysis has been conducted on the tribological behavior of composites that incorporate solid lubricant reinforcements such as h-BN, MoS2, WS2, grapheme, among others. These studies have aimed to explore effects of these reinforcements on friction and wear properties. Additionally, the processing technique used for the fabrication of composites has been investigated, as it plays a crucial role in achieving uniform dispersion, interfacial bonding, and structural stability, all of which ultimately influence the electrical, tribological and mechanical properties of the materials.

Copper has been chosen as the matrix material for synthesis of self lubricating composites due to its wide-ranging applications. Powder metallurgy has proven to be the most suitable method for producing high-quality products in recent decades. Conventional sintering processes, while effective, can be time-consuming. As a result, advanced techniques such as spark plasma sintering (SPS) have gained popularity due to their ability to save time and energy. Based on the information provided, the aim of this study is to fabricate copper matrix composites reinforced with h-BN through various processing techniques and evaluate their tribological performance at both room temperature and 100. The objective of this research is to gain insights into the tribological behavior of these composites, which can contribute to their potential application as materials for future tribological applications.

2 COMPOSITES

Composite materials are characterized as a combination of two or more distinct components that can be physically separated and have different chemical compositions. These composites consist of two or more phases, the matrix, a primary continuous phase, and the reinforcement, a secondary discontinuous phase. There are many elements that can affect a composite's performance and qualities, including:

- The characteristics of the matrix and reinforcing materials.
- The distribution and size of constituents within the composite
- The shape of the constituents
- The nature of interface between the constituents

The main objective behind the development of composites is to achieve desired properties for specific requirements that cannot be attained by monolithic materials alone. These properties may include high hardness, high toughness, improved yield strength, enhanced creep resistance, superior corrosion resistance, improved wear resistance, reduced thermal expansion, and more.

2.1. Types of composites

Composites can be classified based on three main factors: (i) the matrix material, (ii) the reinforcing phase, and (iii) the geometry of the reinforcement.

On basis of the materials of the matrix, composites are categorized as:

- Composites made of metal matrix
- Ceramic matrix composites
- Polymer matrix composites

On the basis of the reinforcing phase, composites are categorized as:

- Fiber reinforcement composites
- Whisker reinforcement composites
- Particulate reinforcement composites

On the basis of the geometry of the reinforcement, composites are categorized as:

- Continuous fiber composites
- Discontinuous fiber composites

2.2: Processing and production of composites

- The production of metal matrix composites involves various approaches, depending on the desired type, number, and distribution of reinforcing components. The selection of process engineering involves considerations such as the choice of particles and fibers as reinforcements, the matrix alloy, and the intended application. Additionally, the processing method is influenced by the initial state of the matrix material. By altering the manufacturing technique, finishing, and processing parameters, as well as the form of the reinforcement components, it is possible to achieve diverse characteristic profiles, even when the composition and quantity of the components remain unchanged.

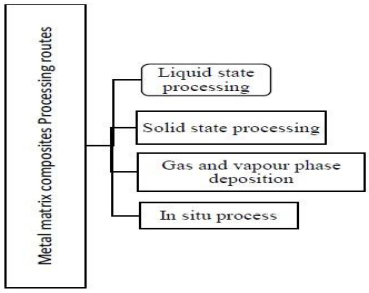

Fig. 2.2: Classification of the processing routes to develop NMC

- As mentioned in Fig. 2.2, metal matrix composite processing routes can be divided into four part as liquid state processing, solid state processing, gas and vapor phase deposition and in situ process.

2.3 Processing of Liquid State

During this process of preparing composites in the state liquid, the reinforcing phase particles are introduced into the molten metal. This mixture is then thoroughly mixed and cast. This liquid state processing can be further classified into three types:

1. Melt stirring technique: In this method, the reinforcing phase is added in molten form and mixed using a stirrer. After appropriate mixing, the mixture is casted to obtain the desired composite.
2. Gas pressure infiltration: In this technique, the reinforcement is infiltrated into a ceramic preform with the assistance of gas pressure. The gas pressure helps in effectively introducing the reinforcing phase into the preform.
3. Squeeze casting: Squeeze casting follows a similar process as gas pressure infiltration. However, the distinction lies in the fact that
4. insqueeze casting, the molten reinforcement is squeezed into the preform using a ram.

2.4 Solid state Processing

In solid state processing, reinforcement is added into solid elemental form. The typical example of this method is Powder metallurgy and diffusion bonding.

(i) Powder metallurgy

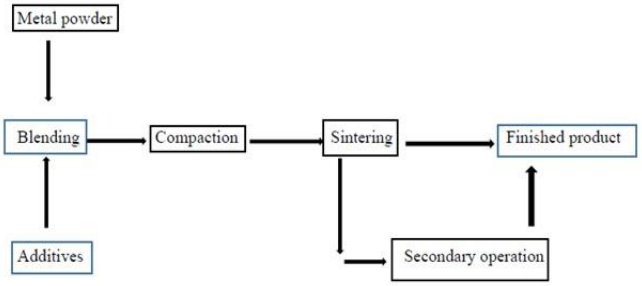

As shown in Fig. 2.3, Powder metallurgy method consists of various sub steps in as specified manner.

Blending: It refers to the process of achieving a uniform mixture of metal powder and additives. During this step, elemental powders, including the matrix and reinforcement materials, are mixed thoroughly using appropriate methods to obtain a secondary powder. Lubricants and other additives may also be incorporated at this stage to minimize friction and wear on the compaction die.

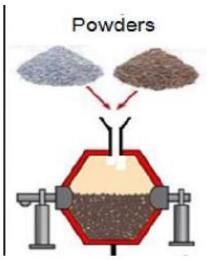

Fig. 2.4. Blending (Hamweendo et.al., 2016)

Compaction: It is the process of compressing the blended powder within a die using an external source of force. When compaction is performed at room temperature, it is referred to as green compaction. The purpose of compaction is to provide strength to the compact through interlocking and plastic deformation. The magnitude of the compaction force is determined by the specific material and its intended application.

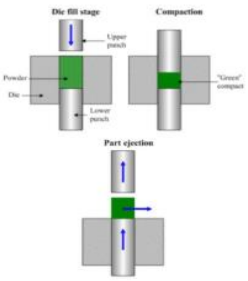

Fig. 2.5 Compaction (Al-Mangour et.al., 2015)

Sintering:

Sintering is a crucial process that involves heating the compacted material to promote particle fusion. This process increases in the density and material strength. Many sintering methods, includes traditional, microwave and spark plasma sintering, have been employed to fabricate composite materials.

In the traditional sintering process, prepared powders are subjected to diffusion heating below their melting point. The duration of this process can range from a few minutes to several hours, allowing for effective bonding between particles.

Microwave sintering, on the other hand, utilizes the dielectric characteristics of the material. These characteristics act as markers for microwave irradiation, facilitating the sintering process.

Hot isostatic pressing is another sintering technique that involves the application of both heat and pressure simultaneously. This technique leads to significant densification of the material.

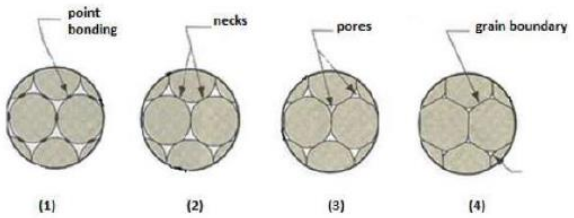

Fig. 2.6 Sintering on microscopic level (Al-Mangour et.al., 2015)

(ii) Diffusion bonding

2.1.2.3 Gas and vapour phase deposition

2.2 Wear and sliding behavior of h-BN

Mahathanabodee et al. (2014) conducted a study highlighting the attractive tribological properties of hexagonal Boron Nitride (h-BN) and its application in the automotive industry, particularly in AA2024 alloy components. The lamellar structure of h-BN, consisting of stacked hexagonal planes with strong covalent bonds between the planes and weak Vander Waals forces, contributes to its solid lubricant characteristics.

O.A. Leoın et al. (2005) found the limitations of h-BN, such as its non-wettability and low sinterability, which can restrict its usability. However, the study also highlighted the advantages of h-BN, including its white color, excellent thermal stability, chemical inertness, and thermal conductivity. These properties make h-BN a promising candidate as a "clean" lubricant, potentially replacing "dirty"

lubricants like graphite or MoS2 in a wider range of lubricant.

Shitang Zhang et al. (2008) conducted a study on The influence of test temperature on the friction and wear behavior of laser cladding Ni/h-BN coating was examined, and the experimental findings demonstrated a substantial impact of temperature on the coating's performance.When sliding against a ceramic counterpart, the coating had a low friction coefficient and wear rate at temperatures up to 800°C.

In the research conducted by Xiuqing Li et al. (2020), the study investigated the tribological performance of B4C/h-BN composite ceramics under dry friction conditions. It found that increasing the applied load led to a gradual decrease in the friction coefficient.

T. Saito et al. (2000) examined The tribological behavior of pure h-BN and sintered h-BN with CaO-B2O3 was investigated in distilled water and saline solution. The study found that the coefficient of friction for pure h-BN sliding on itself in distilled water was 0.06, lower than in air. The presence of a preferentially oriented h-BN transferred film on the steel plate confirmed lamella slip on the h-BN sliding surface.

2.3 Tribology

It includes the investigation of surface interactions caused by relative motion, including friction, wear, and lubrication.In 1967, the Organization for Economic Cooperation and Development (OECD) commission that would later become known as Tribology established the field as a scientific one. The scope of Tribology extends beyond simply reducing friction and wear; its underlying philosophy is to minimize human effort and costs through the adoption of environmentally friendly practices.

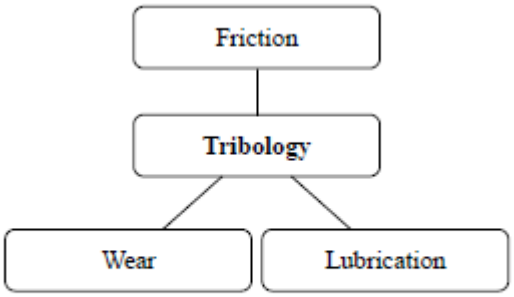

Fig. 2.7 Tribology

Types of wear

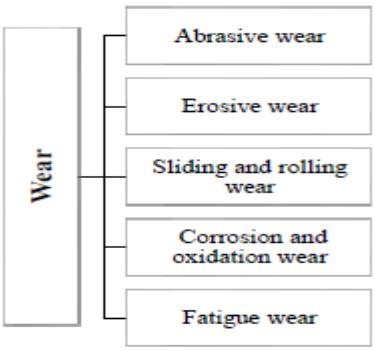

Abrasive wear

It happens when particles of a material of equal or greater hardness come into contact with a solid object. The deterioration of earth-moving machines' shovels is a well-known example of abrasive wear. Be that as it may, the extent of rough wear stretches out past normal insight. Indeed, even materials with a transcendently delicate organization can encounter grating wear on the off chance that they contain hard particles. Due to the small amounts of silica in the plant fibers, organic materials like sugar cane can wear out cane cutters and shredders and cause abrasive wear.

It is essential to keep in mind that the complicated mechanisms involved in the wear process cannot be adequately described by the term "abrasive wear." In terms of controlling and preventing abrasive wear, this presents a significant obstacle. In point of fact, multiple distinct wear mechanisms typically interact with one another, each with its own distinct set of properties.

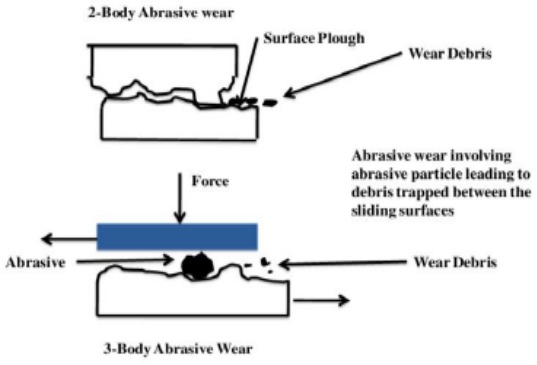

Fig. 2.8-Abrasive wear (Yusoff et.al., 2011)

Sliding wear

Sliding wear means to the relative motion between two smooth solid surfaces under stress, where surface damage

does not occur due to deep grooving caused by asperities or foreign particles during translational sliding. These surfaces can be lubricated or unlubricated, and they can consist of metallic or nonmetallic materials. The friction and wear observed in sliding pairs are influenced by various parameters within the tribosystem, albeit to varying degrees. Wear in sliding contact can be induced by adhesion, surface fatigue, tribochemical reactions, and/or abrasion, and the dominant wear process is determined by several factors.

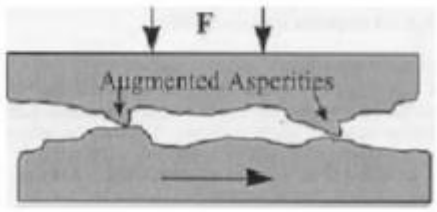

Fig.2.10- Sliding wear (Tanner et.al., 1998)

Wear measurements

1. Wear rate- The term "adhesive wear loss" was coined by Archard in 1953 and according to his expression, The formula states that wear loss is directly proportional to applied stress and inversely proportional to the hardness of the material. One way to put it is as follows:

$$W = \frac{kP}{H} \quad \text{.....(2.1)}$$

where

P = Applied load

W = Wear rate

k = Wear coefficient

H = Hardness of material

2. Wear coefficient- The coefficient mentioned is likely the coefficient of friction, which is a physical parameter used to characterize and correlate the wear behavior of materials.

3. Lubricant analysis- Wear particles in the liquid lubricant can indicate the presence and type of wear in a system, aiding in condition assessment and maintenance activities. Wear particle analysis is a valuable technique for monitoring and predicting component wear.

Prevention of wear
Generally, wear of any material can be prevented by-

• By using wear resistance material

• By keeping the surface apart from each other

• By hardening or chemical modification of material.

2.3.2 Friction

It is a resistance that one body experiences when moving across another. The interaction between the asperities (small protrusions) on the surfaces of two bodies generates the frictional force. The combined resistance offered by all the contact points between the asperities is known as the frictional force. Coulomb proposed three fundamental laws of friction in 1785:

According to the first law, the normal load, or the force pressing the surfaces together, directly proportionately affects friction.

The apparent area of contact between the surfaces has no bearing on the frictional force, according to the second law.

According to the third law, once motion has started, the kinetic frictional force is constant independent of the sliding velocity.

In addition to these laws, other theories of friction have been developed over time. The Adhesion theory of friction, proposed by Bowden and Tabor in 1950, suggests that when two clean surfaces are pressed together at room temperature, strong connections form through cold welding and adhesion. Breaking these junctions requires a force to move one body over the other. Coulomb also proposed the Asperity interlocking theory, which states that surfaces come into contact at specific points called asperities. These asperities bear the applied load and undergo plastic deformation when the load is applied, resulting in frictional resistance.

Another theory, known as the Molecular attraction theory proposed by Hardy in 1931, attributes friction to molecular attraction. This theory is based on the partial irreversibility of the bonding force between atoms. It distinguishes between the real and apparent areas of contact and works over small distances.

The Stick-slip Theory, proposed by Bowden and Leben in 1939, is an alternative theory to adhesion. It suggests that one surface rests on the other at junctions. When sliding occurs, a rise in temperature at these junctions leads to local welding, creating resistance to motion.

2.4 **Formulation of problem**

A critical evaluation of the literature presented above reveals that despite numerous investigations, there is a notable gap in research focusing on multipleCu-based materials with solid lubricants exhibit self-lubricating properties, low friction coefficients, high load-bearing capacity, corrosion resistance, and thermal stability. They

are versatile and find applications in various industries requiring improved tribological performance. In the same proportion but fabricated using different methods. Additionally, there is limited exploration on the combined utilization of solid lubricants such as MoS2 and h-BN, which may synergistically reduce friction and provide effective lubrication across various operating conditions, including load, speed, and temperature.

Based on the aforementioned observations, the present study aims To investigate tribological behavior, experiments are conducted to study friction, wear, and lubrication characteristics. The goal is to understand material response, optimize performance, and identify suitable lubrication methods innovative copper-based composites incorporating h-BN and functionalized h-BN in equal quantities, but produced using different manufacturing parameters. Furthermore, the study aims to assess the influence of various manufacturing parameters on the tribological properties of these composites.

2.5 **Objectives of study**

In consideration of the aforementioned points, the current study has been conducted with the primary objectives:

i. To employ the powder metallurgy technique and spark plasma sintering to fabricate Cu-h-BN composites with variations in sintering parameters, as detailed in the subsequent chapter.

ii. To investigate the wear and friction characteristics of these composites at about 20 to 25 degrees Celsius and elevated temperatures, specifically under constant load and constant sliding velocity condition

EXPERIMENTAL PROCEDURE

This chapter provides comprehensive information regarding the acquisition of materials, along with a detailed description of the experimental procedures employed in the synthesis of copper-h-BN composites. It also outlines the characterization methods utilized for evaluating the friction and wear behavior of the composites, as well as the techniques employed for analyzing the samples and worn surfaces.

3.1 Selection and procurement of material

The raw materials used in present study are powders of Cu (325 mesh, 99.5% purity) and hexagonal boron nitride (70 nm)

3.2 Synthesis of composites

3.2.1 Mixing of powder

The experimental procedure commenced by accurately weighing the required amounts of metal powders using a precise electronic balance with a sensitivity of 0.0001g. Subsequently, the powders were thoroughly mixed in the desired ratios using a combination of a pestle and mortar, as well as ball milling for a duration of 4 hours. The mixing process was performed for four different composites, all under the same parameters.

3.2.2 Spark plasma sintering

The thoroughly milled composites were subsequently subjected to spark plasma sintering using the Dr. Sinter SPS-625 equipment from Fuji Electronic Industrial Co. Ltd. (Japan) at IIT Roorkee. The sintering process was conducted under the following parameters: a pressure of 40 MPa, a sintering temperature of 850˚C, a heating rate of 100˚C/min, and a holding time of 5 minutes. The aim of employing different processing techniques for the fabrication of three distinct Cu-h-BN composites was to achieve a tough bonding between the matrix and reinforcement phases, thereby anticipating a reduction in friction and wear. The variations in the processing techniques for these composites are as follows:

I. CB: Hexagonal boron nitride was added to copper powder and thoroughly mixed using a combination of a pestle and mortar, as well as ball milling for 4 hours. Subsequently, the mixture underwent the SPS process.

II. CBC: Functionalized boron nitride was mixed with copper powder using a pestle and mortar, followed by ball milling for 4 hours. The mixture was then subjected to the SPS process.

III. CBCP: Functionalized boron nitride was mixed with copper powder using a pestle and mortar, followed by ball milling for 4 hours. Subsequently, the mixture underwent a pre-sintering step in a nitrogen atmosphere at 950˚C using a tube furnace for a duration of 2 hours. The processed material formed hard lumps, which were crushed and further ball milled for 6 hours to restore it to a powder form. The obtained mixture was then fabricated using the SPS technique.

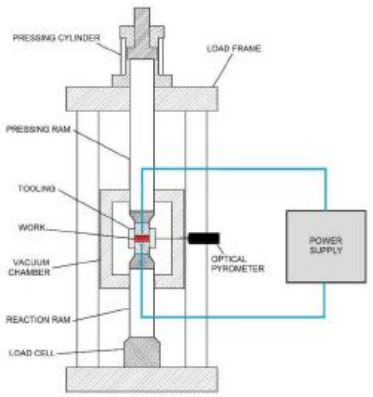

Fig. 3.1 Schematic diagram of a spark plasma sintering machine (Zhao Hui Zhang et.al., 2014)

Table 3.1**Composition, designation and sintering parameters of materials synthesized**

Designation			
C	0	40	850
CB	2	40	850
CBCP	2	40	850

3.3 Characterization of h-BN and h-BN-Cu Composites

The powders of h-BN-Cu were exposed to several characterization procedures in order to check the shape, composition, and chemical structures of the created hybrid materials.

3.3.1 X-Ray diffraction analysis

Through the utilization of X-ray diffraction analysis, the presence of metals and compounds in the samples was verified. This technique allowed for the identification of the crystallographic planes on which specific compounds or elements were present. Figure 3.2 illustrates the diffraction of X-rays by a crystal, with X-rays employing electromagnetic waves characterized by wavelengths on the order of 1 Å. The use of X-rays is particularly suitable for examining the structure of crystal lattices, Wave diffraction happens when the diffracting object's dimensions are similar to wave.

To generate X-rays, an X-ray tube was employed as an X-ray generator. The X-ray tube had a water-cooled copper target for directing an accelerated electron beam with energies up to a few tens of keV, all within a vacuum tube. This phenomenon resulted in the emission of X-rays with wavelengths typical of the element aluminum. Inelastic interactions produced X-rays with energies up to the energy of the electron beam.

The interference of diffracted waves from different atoms played a significant role in determining the intensity distributions observed. The resulting intensity distributions were greatly influenced by this interference. When atoms are arranged periodically in crystals, the resulting diffracted waves display distinct interference maxima or peaks, which exhibit the same symmetry as the distribution of atoms. By analyzing the diffraction pattern, it becomes feasible to determine the arrangement of atoms within a given material. This technique allows for the investigation of the atomic structure and provides valuable insights into the crystal lattice and the spatial organization of atoms. Through diffraction analysis, scientists can gain a deeper understanding material properties and behavior advances fields like materials science, chemistry, and solid-state physics, driving innovation and enabling improved materials and technologies

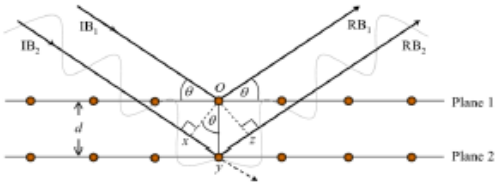

Fig. 3.2 Schematic of diffraction of X-ray (Evan Lyle Thomas et.al., 2006)

Peaks in the X-ray diffraction pattern correspond to the spacing between atoms in a crystal lattice. Bragg's law enables the calculation of diffraction conditions for a peak using the interplanar distance d: $2d\sin\theta = n\lambda$, where θ is the incident angle, λ is the X-ray wavelength, and n is an integer indicating the peak's order. This formula allows scientists to determine the interatomic distances and crystal structures by analyzing the diffraction pattern. Bragg's law is a fundamental principle in X-ray crystallography and plays a crucial role in elucidating the atomic arrangements within materials.

In this study, X-ray diffraction (XRD) analysis was conducted using an XPert PRO instrument (PANalytical) equipped with a graphite monochromator and Coca radiation. The XPert PRO automatically scanned the diffraction pattern within the angle range (2θ) of 0° to 90°. By inputting the components used in the casting process, the XRD analysis could automatically detect the various compounds formed, which were then observed as distinct peaks in the obtained diffraction pattern.

3.3.2 Scanning electron microscopy

A focussed electron beam was used in scanning electron microscopy (SEM) to take pictures of the sample surface.This imaging technique involves the interaction of electrons with the atoms

present in the sample, resulting in the generation of a signal that carries surface topography information. A raster scan pattern is utilized to systematically scan the electron beam across the surface, and the position of the beam is combined with the intensity of the detected signal to create an image representation.

To ensure accurate imaging and prevent any disturbances, the SEM procedure is conducted under vacuum conditions. This is necessary because the presence of air can cause the electron beam's trajectory to deviate, consequently altering the surface topography observed. By maintaining a vacuum environment, the integrity and accuracy of the SEM imaging process are preserved.

3.4 Measurement of Hardness

The hardness of a material is determined using Vickers method, which involves applying a load of 300 g for a

duration of 10 seconds. When subjected to forces like indentation, scraping, and rebound, a material's ability to resist permanent deformation is measured by its hardness. In the Vickers test, a 136° pyramid-shaped indenter is used to create an indentation on the material's surface.

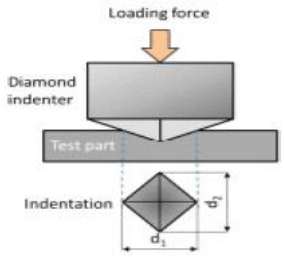

Fig. 3.3 Schematic of Vicker's hardness (Dragon Adamovic et.al., 2021)

Where, HV = Vicker's hardness value

F = applied load

d = average of d1 and d2

3.5 Density measurement

Archimedes' law is used to estimate density. In this procedure, the sample's mass is first measured in the air and then in the water.

Let,

m1= Mass of sample in air

m2= Mass of sample in water

ρ = Density of water

$$\text{Density of sample} = \frac{m1}{m1-m2}\rho \quad \ldots\ldots\ldots\ldots\ldots\ldots\ldots\ldots(3.1)$$

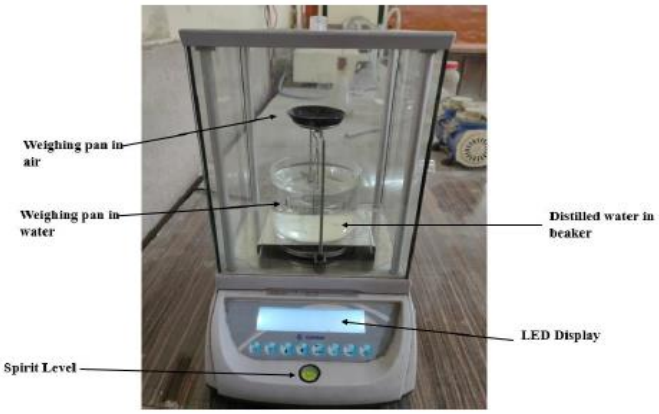

Fig.3.4 Density balance

3.6 Friction and wear testing

Dry sliding wear tests were conducted on pure copper and the composites following the guidelines of ASTM standard 133. A ball-on-disc rotary tribometer was used for the tests, and an image of the machine can be seen in Figure 3.5.

During wear test, the tangent force were continuously monitored, and the data was recorded using the tribometer's accompanying PC. By dividing the friction force by the applied normal load, the friction coefficient was calculated. In this particular experiment, only pre-calibrated dead loads were used.

A flexible tool, the ball-on-disc machine can be used to assess the wear and friction characteristics of various materials under lubricated and non-lubricated situations.The test involves sliding friction between a stationary ball stylus and a rotating disc. The wear track diameter, normal load, and rotational speed can be adjusted as needed.

In the ball-on-disc test, wear is determined by pressing a ball onto a rotating disc under a defined force. The ball has a radius added to its top, resulting in a point contact between the ball and the disc at the beginning of the test. As the test progresses, the contact area gradually expands. It is important to note that there was no reversing motion or interruption of the lubricating film observed.

Fig. 3.5. Ball on disc tribometer

Table 3.2 Tribological testing parameters

Composition	Load	Sliding Speed (m/s)	Temperature	Number of Cycles
C	3	0.3	Room temp, 400	10000
CB	3	0.3	Room temp, 400	10000
CBC	3	0.31	Room temp, 400	10000
CBCP	3	0.3	Room temp, 400	10000

Calculations of the coefficient of friction and wear rate are made following the tribo test. Friction Coefficient is ratio of sliding force to normal force acting on sample and wear rate is ratio of volume loss to sliding distance. Same is shown by following equations-

Let N = normal force applied by ball on sample

F = sliding force generated on sample

$$\text{Coefficient of friction} = \frac{F}{N} \quad \text{.....(3.2)}$$

And

$$W = \frac{\textit{Volume loss}}{\textit{Sliding distance}} = \frac{Ap \times \pi D}{\pi DN} \quad mm^3.m^{-1} = \frac{(mi-mf)}{\varrho} / L \quad \text{.....(3.3)}$$

Where, W = Wear rate

Ap = Area of profile

D = Diameter of wear track

N = Number of cycles

3.7 Characterization of worn surface

Each sample's worn surfaces were meticulously analyzed using a scanning electron microscope (SEM) to determine the main wear mechanisms. Additionally, the worn surface of the counter face balls and the wear debris were also analyzed using SEM. Two SEM instruments were utilized for surface examination: the FEI Nova Nano SEM and the EVO-18 Carl ZEISS. The choice of instrument depended on the specific resolution and magnification requirements of the analysis.

RESULT AND DISCUSSION

This chapter describes the results on the X-ray diffraction microstructural characterization of Cu-h-BN composites. The results on density and hardness of the composites are also presented along with the results on dry sliding friction and wear behavior of the composites.

4.1 Surface Characterization

4.1.1 X-Ray diffraction analysis

The initial examination conducted was X-ray diffraction analysis, which provided confirmation of the presence of Cu, BN, and other formed compounds in the composites. Figure 4.1(a through c) illustrates the XRD patterns of Cu-h-BN composites. In all three composites (CB, CBC, CBCP), characteristic peaks correspond to copper (JCPDS card no. 000031005 and 000040836) were observed. Specifically, the peak at 2θ of 73.997° corresponding to the (220) plane and the peak at 2θ of 94.38° corresponding to the (222) plane of copper were present. Additionally, other peaks were identified as being attributed to the presence of boron nitride, with JCPDS card numbers 000260773, 000450894, and 000260773, appearing at 2θ of 42.739°, 50.079°, and 89.62°, respectively, corresponding to the (002), (102), and (112) planes.

No additional peaks were observed in any of the composites, indicating that all constituent components were present in their original form within the composites. Figure 4.1(d) displays the XRD pattern of h-BN powder, where peaks corresponding to BN (JCPDS numbers 000340421 and 010732095) were identified at 2θ values of 23.08°, 26.765°, 32.125°, 41.598°, 50.15°, 55.165°, 75.934°, and 82.187°, corresponding to the (020), (002), (112), (100), (102), (004), (110), and (112) planes, respectively. Furthermore, the presence of boron (JCPDS number 000310207) was also detected at 2θ values of 34.38° and 39.159°, corresponding to the (131) and (315) planes, respectively.

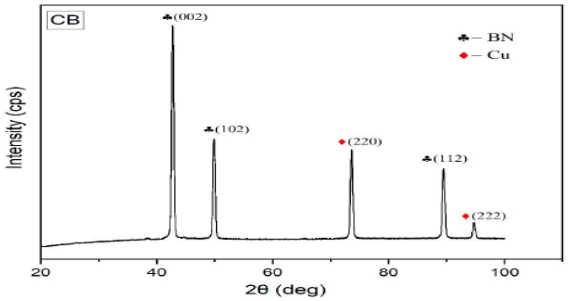

(a)

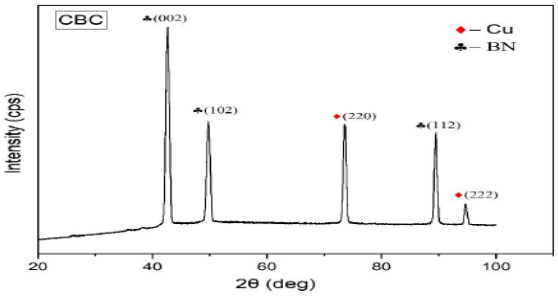

(b)

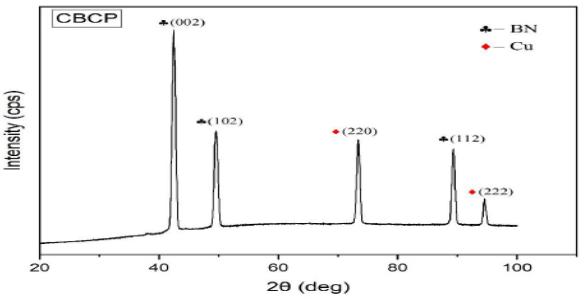

(C)

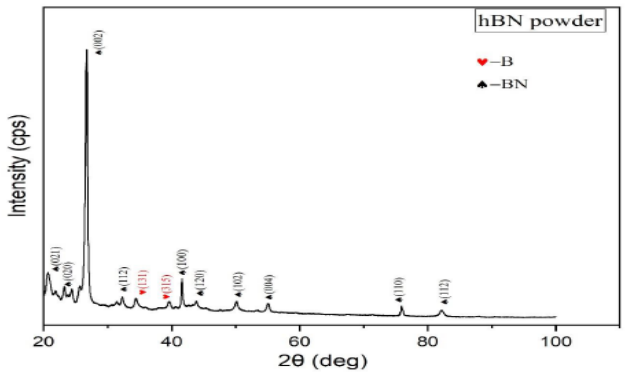

(d)

Fig. 4.1 X-Ray diffraction graph of (a) CB, (b) CBC, (c) CBCP, (d) h-BN powder

4.1.2 Scanning electron microscopy analysis

SEM micrographs depicting the microstructure of the composites CB, CBCP, and CBC are displayed in Figure 4.2 (a through c). In Figure 4.2 (a), the microstructure of CB is presented, revealing the dispersion of h-BN particles alongside the presence of pores or voids [5]. Similarly, Figure 4.2 (b) displays the microstructure of CBC, indicating the dispersion of h-BN particles along with some pores. Figure 4.2 (c) exhibits a higher number of voids compared to CB and CBC. This disparity is attributed to the formation of hard lumps in the case of CBCP.

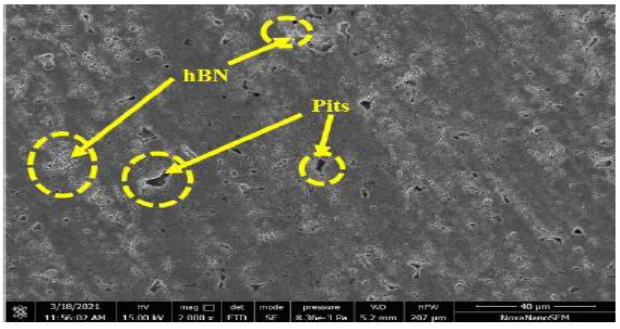

Fig 4.2(a) SEM image of composite CB

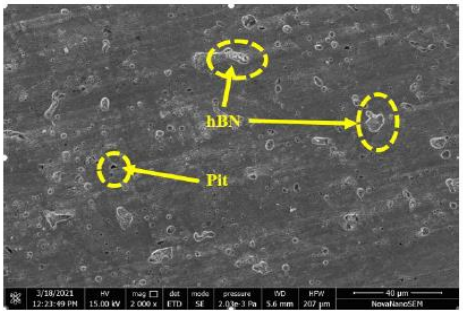

Fig 4.2(b) SEM image of composite CBC

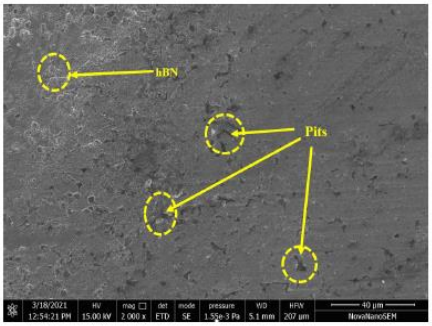

Fig. 4.2 (c) SEM image of composite CBCP

Figure 4.3 depicts the micrographs were accompanied by the corresponding area. Presence of C, B, N, O and Cu in the elemental mapping corresponding to composites shows that the composite contains h-BN and copper. From elemental mapping, we can also get approximate amount of each present element.

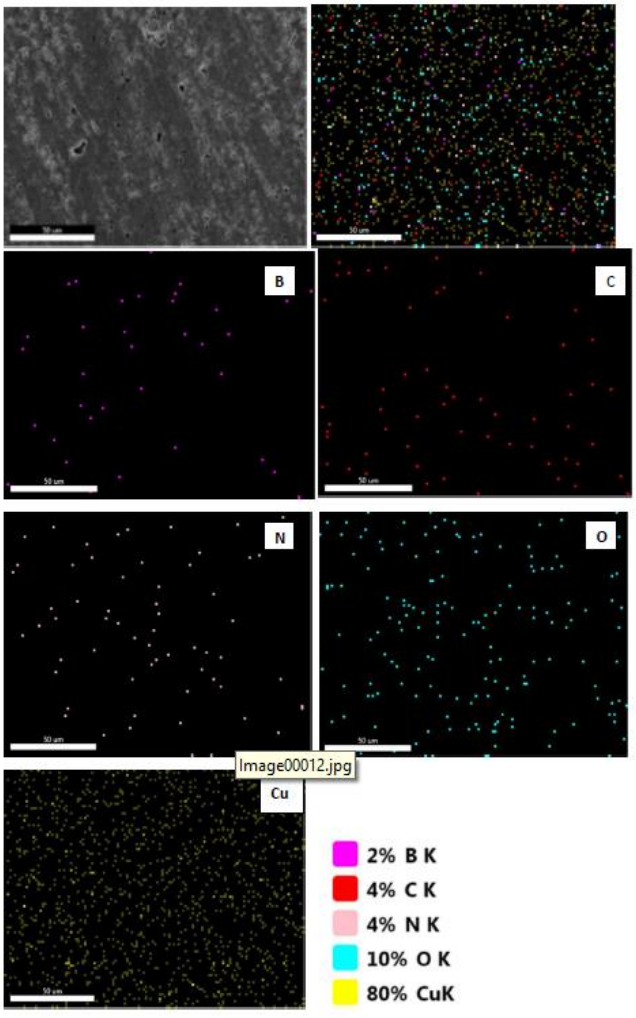

Fig.4.3(a) Elemental mapping of composite CB

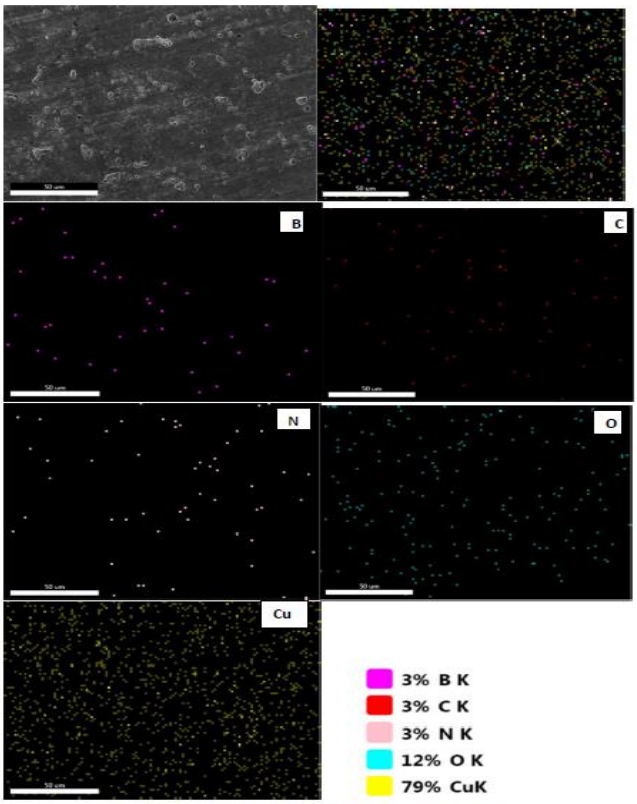

Fig.4.3(b) Elemental mapping of composite CBC

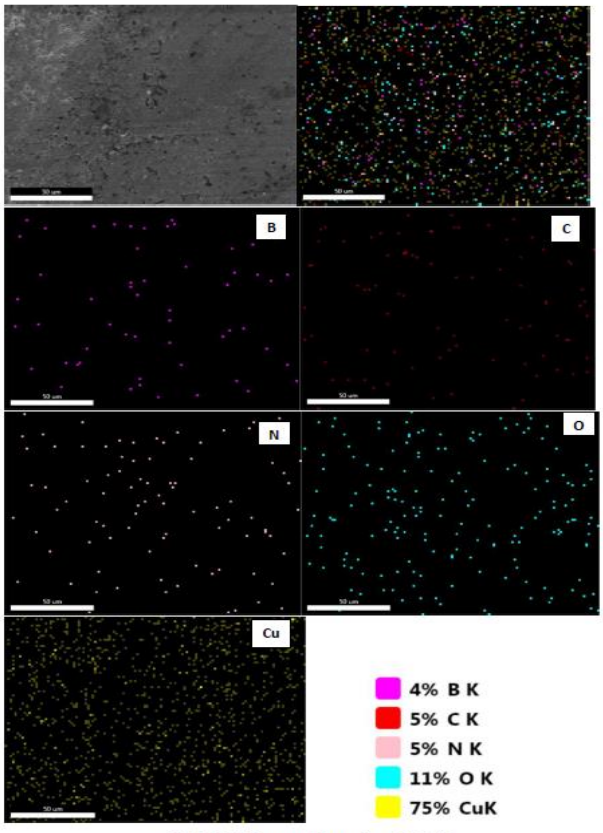

Fig.4.3(c) Elemental mapping of CBCP

4.2 Density measurement

Table 4.1 provides the density values of pure copper and Cu-h-BN composites, including theoretical densities, actual densities, and relative densities. Among all the materials studied in this research, the pure copper sample exhibits the highest density as well as relative density. On the other hand, composite CB demonstrates the lowest density, while composite CBC exhibits the highest density among the composites. The table shows that the composites' densities are lower than those of pure copper. This behavior can be seen to presence of less dense h-BN reinforcement in the composites. All density measurements were performed using the Archimedes principle.

Table 4.1. Deasity of copper and composites

Composition			
	8.406	8.58	92.67
	6.899	8.32	84.88
	8.040	8.38	88.78
	7.496	8.39	90.25

4.3 Hardness measurement

Figure 4.5 displays the indentations made by a diamond pyramid on the samples. Upon examination, it is evident that the diagonal of the indentation shape is largest in composite CB and smallest in pure copper. This indicates that the projected area of the indentation is largest for composite CB and smallest for pure copper, resulting in the minimum hardness for CB and maximum hardness for pure copper, considering the same applied load of 200 g. Likewise, similar observations can be made for the other composites.

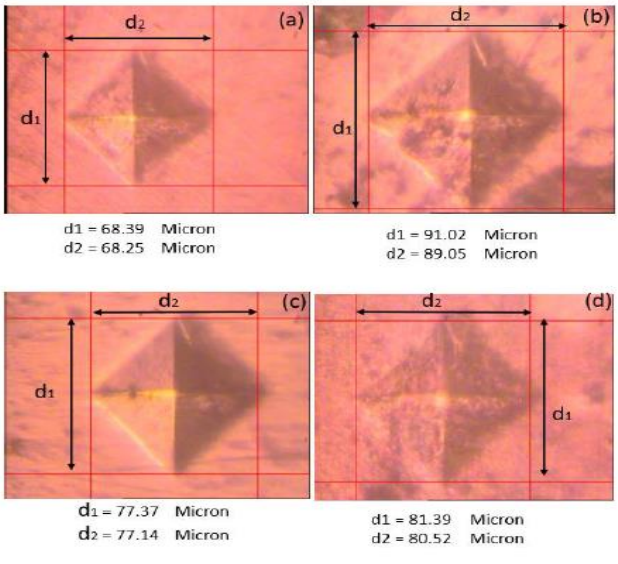

Fig. 4.5 Vickers diamond indentation image on (a) C (b) CB (c) CBC (d) CBCP

4.4 Friction and Wear behavior

Figure 4.6 presents a comparison of the friction coefficient and cyclic contacts for copper and Cu-based composites under specific test conditions. The friction profiles of pure copper, CB, and CBC composites remain consistent, while the CBCP composite shows significant variation. Initially, the CBCP composite exhibits a low friction coefficient (< 0.2) for the first 4000 cycles, followed by a sudden increase and eventual stabilization at around 0.6. Importantly, the CBC composite consistently displays the lowest friction coefficient throughout the test duration.

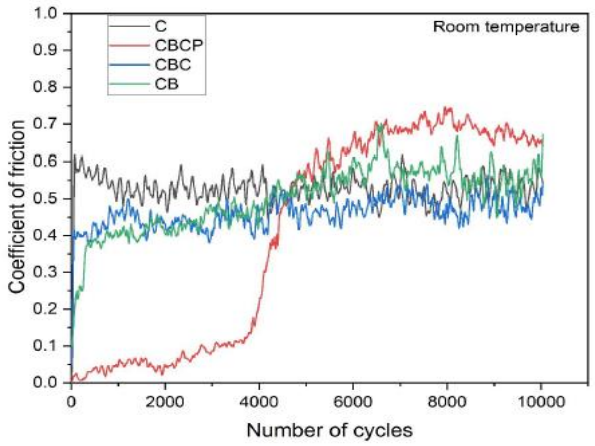

Fig 4.6 Variation of coefficient of friction with number of cycles at room temperature

Figure 4.7 demonstrates the connection between the friction coefficient and the number of cycle contacts at 100°C, 3 N of load, and 0.3 m/s of sliding speed. Similar to the behavior observed at room temperature, all composites and pure copper demonstrate stable friction profiles. However, there are notable differences in the friction characteristics among the materials. Pure copper exhibits a relatively higher friction coefficient compared to the composites. The CBC composite, on the other hand, has a lower coefficient of friction when compared to the other materials.

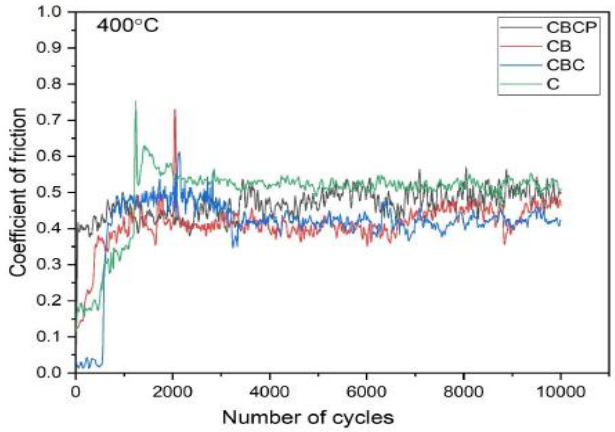

Figure 4.8 depicts the variations in the average coefficient of friction for different compositions and temperatures, including pure copper. The results shows that average coefficient of friction is higher at room temperature in comparison to the measurements recorded at 400°C. Among the samples tested, the composite CBC exhibits the lowest coefficient of friction, while pure copper demonstrates the highest friction coefficient. Furthermore, friction coefficient for CBCP composite is found to be higher than that of the CBC composite.

Figure 4.9 depicts the fluctuations in the wear rate for the copper and composite concerning composition and temperature. Composite CB exhibits the highest wear rate among all the samples, which can be attributed to its lower hardness and density. Conversely, pure copper demonstrates the lowest wear rate, likely due to its higher hardness and density. It is notable that pure copper, CB, and CBC display higher wear rates at the temperature about 20 to 25 degreecelcius compared to those observed at 100°C. However, the CBCP composite shows the opposite trend, with a lower wear rate at room temperature and a higher wear rate at 100°C.

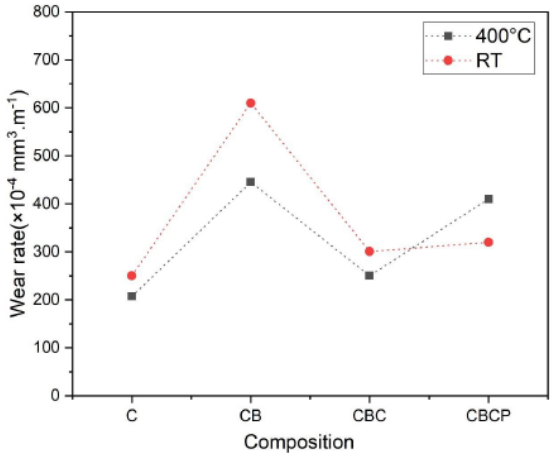

Fig 4.9 Variation of wear rate with composition and temperature

4.5 Worn surface analysis

The worn surfaces and wear tracks of pure copper and composites CB, CBC, and CBCP have been observed under SEM at different magnifications to study their morphological features and understand the examined friction and wear behavior. In Figure 4.9 (a-e), SEM micrographs of the worn surfaces are presented for samples tested at room temperature, with a load of 3 N and a sliding speed of 0.3 m/s.

Figure 4.9 (a) shows the worn surface of copper at at the temperature about 20 to 25 degreecelcius. Delamination and the presence of a compact layer can be observed in certain areas.

Figure 4.9 (b) displays the worn surface micrograph of composite CB tested at room temperature. Fine debris is observed in some regions of the worn surface, along with deep grooves, ploughing, and pits.

Similarly, Figure 4.9 (c) shows the worn surface micrograph of composite CBC tested at room temperature. Delaminating and pouching are evident on the worn surface.

Figure 4.9 (d) presents the worn surface micrograph of composite CBCP tested at room temperature. This micrograph reveals the presence of particle-like debris, embedded debris, and ribbon-like debris on the worn surface. Only embedded debris is observed in this case.

To gain further insight, the surface morphology of the EN 31 ball of steel used as a counter face against composite CBC (which exhibits the minimum coefficient of friction) is also examined. Figure 4.9 (e) shows the micrograph of the counter face, indicating the presence of a transfer layer of debris.

These SEM observations provide valuable information about the surface characteristics and wear mechanisms, aiding in the interpretation of the friction and wear behavior of the materials studied.

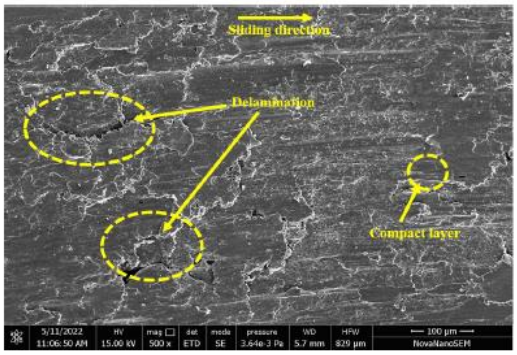

Fig. 4.10 (a) SEM micrograph of worn surface of pure copper at room temperature

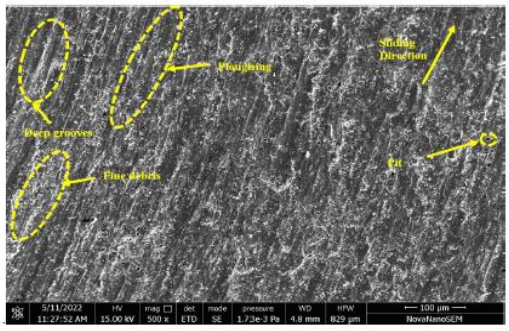

Fig. 4.10 (b) SEM micrograph of worn surface of composites CB at room temperature

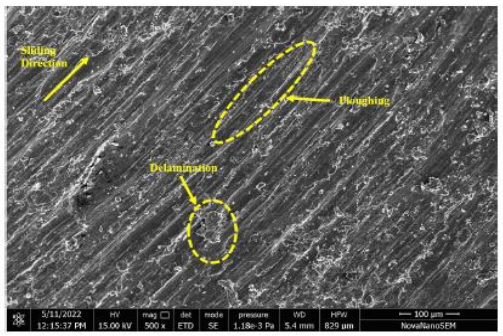

Fig. 4.10(c) SEM micrograph of worn surface of composites CBC at room temperature

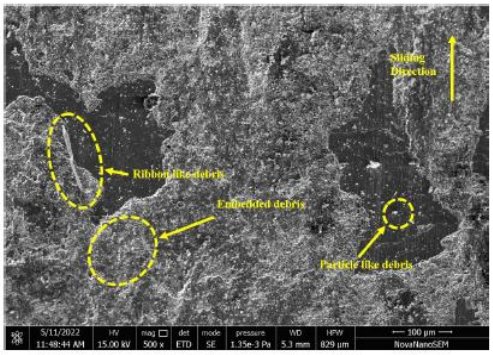

Fig. 4.10(d) SEM micrograph of worn surface of composites CBCP at room temperature

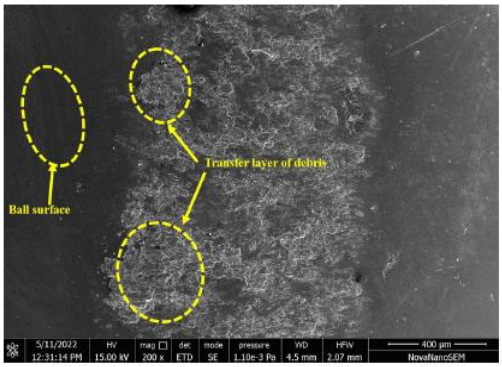

Fig. 4.10(e) SEM micrograph of EN 31 ball used against CBC at room temperature

The worn surfaces and wear tracks of samples tested at 400°C have also been observed under SEM at different magnifications to study their morphological features and understand the observed friction and wear behavior. Figure 4.10 (a-d) present the SEM micrographs of the worn surfaces for pure copper and composites CB, CBC, and CBCP tested at 400°C.

In Figure 4.10 (a), the SEM micrograph shows the worn surface of pure copper at 400°C. Bright patches on the surface indicate the occurrence of oxidation.

Figure 4.10 (b) displays the SEM micrograph of the worn surface of composite CB tested at 400°C. Features such as pits, delamination, and ploughing are visible, suggesting different wear events taking place in this composite.

In the case of composite CBC, as shown in Figure 4.10 (c), delamination is observed to be a significant wear event on the worn surface. Ploughing and other features may also be present.

Figure 4.10 (d) presents the SEM micrograph of the worn surface of composite CBCP tested at 400°C. Delaminating is again observed as a major wear event, and debris particles can be seen on the surface.

By examining these micrographs, important wear mechanisms and surface characteristics can be identified, contributing to the observed wear and friction behavior in materials at elevated temperatures.

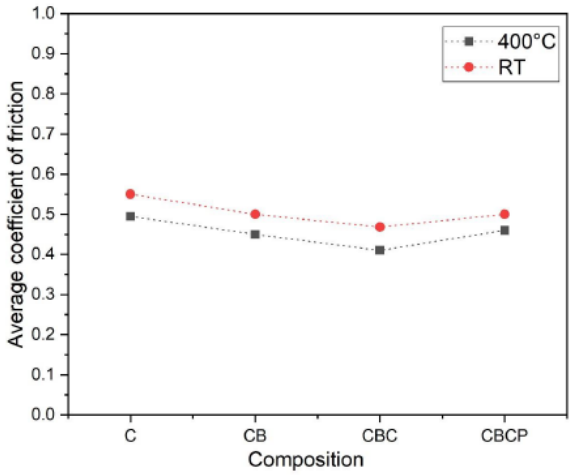

Fig 4.8 Variation of average coefficient of friction with composition and temperature

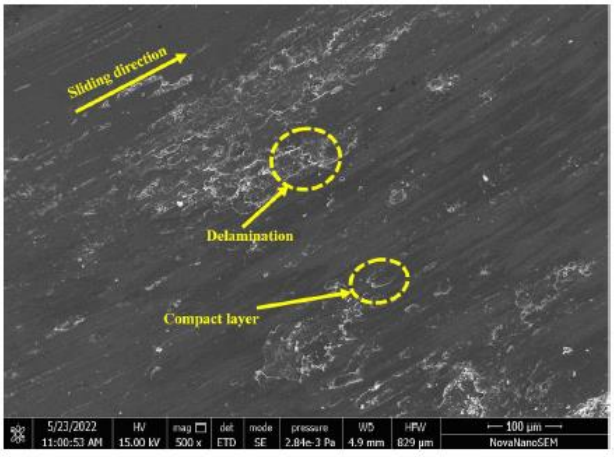

Fig. 4.11 (a) SEM micrograph of worn surface of pure copper at 400°C

Figure 4.10 (e) displays the SEM micrographs of the EN 31 balls of steels used as the counter face and slid against the CBC composite.. The micrographs reveal the presence of adhered material on the surface of the steel ball, indicating that material from the composite CBC has been transferred onto the counter face. This observation suggests that there is a transfer of material between the composite and the counter face during the sliding process.

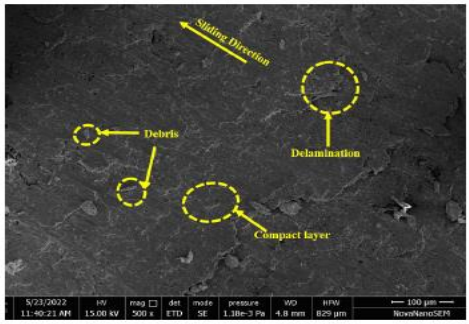

Fig. 4.11 (d) SEM micrograph of worn surface of composites CBCP at 400°C

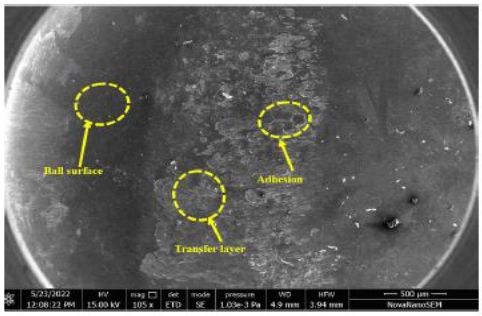

Fig. 4.11(e) SEM micrograph of EN 31 ball used against CBC at 400°C

4.6 Discussion

X-ray diffraction analysis, as shown in Figure 4.1(a-d), confirms the presence of h-BN, copper, and other formed compounds in the composites. No additional peaks were observed in the composites, indicating that all constituent components are present in their original form. The microstructure of each composite, depicted in Figure 4.2(a-c), shows a relatively uniform distribution of h-BN particles in copper, along with the presence of pores/voids [5]. Composite CBCP exhibits a greater number of pores compared to the other composites, which can be attributed to the production method employed and poor sintering.

The hardness of the composites is reduced compared to pure copper, as evident from Figure 4.4. Among the composites, CBC exhibits the highest hardness due to the presence of copper as a functional group in functionalized h-BN, which enhances the sintering ability. On the other hand, CB exhibits the lowest hardness because pure h-BN lacks any functionalized group to enhance sintering. The density of the

composites is also lower than that of pure copper due to the lower density of h-BN (2.1 g/cm3) compared to pure copper (8.9 g/cm3), as well as the poor sintering ability leading to porosity.

Figure 4.6 illustrates that pure copper, CB, and CBC composites exhibit stable friction profiles, while CBCP composites show the number of cycles at room temperature. Among the stable profiles, composite CBC consistently displays the lowest friction coefficient throughout the analysis. The presence of functionalized h-BN in composite CBC may contribute to this behavior by acting as a self-lubricant. This trend is also observed at 400°C, where the coefficient of friction remains lower due to the effective lubricating properties of h-BN at higher temperatures (typically above 200°C) [6].

In Figure 4.9, the wear rate of the composites is compared with pure copper, and it is found that composite CB has the highest wear rate among all samples. This can be attributed to the low hardness and low density of composite CB. On the other hand, pure copper exhibits the lowest wear rate, thanks to its high hardness and density. Additionally, it can be observed that the wear rate is lower at 400°C compared to room temperature. This can be explaine by examining the worn surface micrographs shown in Figure 4.11(a-d), where the adhesion of debris is more pronounced at higher temperatures, filling the surface and reducing the wear rate.

CONCLUSIONS AND FUTURE SCOPE

This chapter provides a summary of the key findings from the current investigation on the tribological performance of pure copper and copper-based composites reinforced with h-BN. Additionally, the chapter also discusses the future scope of research based on the results of this investigation.

Following are the conclusions from the study:

1. X-ray diffraction analysis confirmed the presence of copper, h-BN, and other formed compounds in the composites. No additional peaks were observed, indicating that all constituent components were present in their original form.

2. The microstructure analysis using SEM revealed an equal distribution of h-BN particles in copper matrix in all composites. Pores/voids were also observed, with the highest number of voids found in composite CBCP due to the method of production and poor sintering.

3. The hardness of the composites was lower compared to pure copper. This reduction in hardness can be attributed to the bad sintering behavior of h-BN. Composite CBC exhibited the highest hardness among the composites due to the presence of copper as a functional group in functionalized h-BN, which enhanced the sintering ability.

4. Because h-BN has a lower density than pure copper, the composites have a lower density than pure copper. Poor sintering ability also contributed to the lower density of the composites.

5. The friction behavior of the composites varied with the number of cyclic contacts. Composite CBC exhibited the most stable friction profile, while CBCP showed significant variation in friction. The presence of functionalized h-BN in CBC may contribute to the lower friction coefficient.

6. The temperature and the composition of the composites both had an impact on how quickly they wore down. Composite CB had the highest wear rate, attributed to its low hardness and density. Pure copper exhibited the lowest wear rate due to its higher hardness and density. At 400°C, the wear rate was lower compared to room temperature, which could be explained by the adhesion of debris filling the surface at higher temperatures.

5.1 Future scope

In terms of future scope, based on the findings of the current study, several areas of further research can be explored. These include:

1. Investigating the effect of different reinforcement materials and their combinations with h-BN on the tribological properties of copper-based composites.

2. Studying the influence of various processing techniques and parameters on the microstructure, mechanical properties, and tribological performance of copper-based composites.

3. Exploring alternative methods for improving the sintering behavior of h-BN in composites to enhance their hardness, density, and wear resistance.

4. Conducting in-depth analysis and characterization of the worn surfaces using advanced techniques such as atomic force microscopy (AFM) and transmission electron microscopy (TEM) to gain a deeper understanding of the wear mechanisms and surface interactions.

5. Investigating the long-term durability and performance of copper-based composites in real-world applications, considering factors such as cyclic loading, temperature variations, and environmental conditions.

REFERENCES

1. Nautiyal, H., Kumari, S., Khatri, O. P., & Tyagi, R. (2019). Copper matrix composites reinforced by rGO-MoS2 hybrid: Strengthening effect to enhancement of tribological properties. Composites Part B: Engineering, 173, 106931.

2. Nautiyal, H., Kumari, S., Rao, U. S., Tyagi, R., & Khatri, O. P. (2020). Tribological performance of Cu–rGO–MoS2 nanocomposites under dry sliding. Tribology Letters, 68(1), 1-14.

3. Mahathanabodee, S., Palathai, T., Raadnui, S., Tongsri, R., &Sombatsompop, N. (2014). Dry sliding wear behaviour of SS316L composites containing h-BN and MoS2 solid lubricants. Wear, 316(1-2), 37-48.

4. Kimura Y., Wakabayashi, T., Okada, K., Wada, T., & Nishikawa, H. (1999). Boron nitride as a lubricant additive. Wear, 232(2), 199-206.

5. Niu, W., Sun, R. L., & Lei, Y. W. (2011). Effect of h-BN content on microstructures of the laser cladding self-lubricant coatings. In Advanced Materials Research (Vol. 154, pp. 609-612). Trans Tech Publications Ltd.

6. Zhang, S., Zhou, J., Guo, B., Zhou, H., Pu, Y., & Chen, J. (2008). Friction and wear behaviour of laser cladding Ni/h-BN self-lubricating composite coating. Materials Science and Engineering: A, 491(1-2), 47-54.

7. Saito, T., & Honda, F. (2000). Low friction behaviour of sintered h-BN sliding in sodium chloride solution. Wear, 244(1-2), 132-139.

8. Xu, E., Huang, J., Li, Y., Zhu, Z., Cheng, M., Li, D., ... & Jiang, Y. (2019). Graphite cluster/copper-based powder metallurgy composite for pantograph slider with well-behaved mechanical and wear performance. Powder Technology, 344, 551-560.

9. Kovalčíková, A., Balko, J., Balázsi, C., Hvizdoš, P., &Dusza, J. (2014). Influence of h-BN content on mechanical and tribological properties of Si3N4/BN ceramic composites. Journal of the European Ceramic Society, 34(14), 3319-3328.

10. Li, X., Gao, Y., Wei, S., Yang, Q., & Zhong, Z. (2017). Dry sliding tribological properties of self-mated couples of B4C-h-BN ceramic composites. Ceramics International, 43(1), 162-166.

11. Kushwah, R., Jayan, M. S., Kanagasabapathy, H., Kumar, T. C. A., Halder, S., Begum, N., & Rajkumar, S. (2021). The impact of boron nitride (BN) on tribological behaviour of AZ84 magnesium matrix composites. Materials Today: Proceedings.

12. Elkady, O. A., Abu-Oqail, A., Ewais, E. M., & El-Sheikh, M. (2015). Physico-mechanical and tribological properties of Cu/h-BN nanocomposites synthesized by PM route. Journal of Alloys and Compounds, 625, 309-317.

13. Dash, K., Ray, B. C., &Chaira, D. (2012). Synthesis and characterization of copper–alumina metal matrix composite by conventional and spark plasma sintering. Journal of Alloys and compounds, 516, 78-84.

14. Qin, H., Liang, Y., & Huang, J. (2021). Size and temperature effect on the mechanical properties of graphene/hexagonal boron nitride Van der Waals heterostructure. Materials Science and Engineering: B, 265, 115006.

15. Roy, S., Zhang, X., Puthirath, A. B., Meiyazhagan, A., Bhattacharyya, S., Rahman, M. M., ... &Ajayan, P. M. (2021). Structure, Properties and Applications of Two-Dimensional Hexagonal Boron Nitride. Advanced Materials, 33(44), 2101589.

16. Shu, R., Jiang, X., Liu, W., Shao, Z., Song, T., & Luo, Z. (2019). Synergetic effect of nano-carbon and h-BN on microstructure and mechanical properties of Cu/Ti3SiC2/C nanocomposites. Materials Science and Engineering: A, 755, 128-137.

17. Majety, S., Cao, X. K., Dahal, R., Pantha, B. N., Li, J., Lin, J. Y., & Jiang, H. X. (2012, January). Semiconducting hexagonal boron nitride for deep ultraviolet photonics. In Quantum Sensing and Nanophotonic Devices IX (Vol. 8268, pp. 607-614). SPIE.

18. Thachnatharen, N., Khalid, M., Arulraj, A., &Sridewi, N. (2022). Tribological performance of hexagonal boron nitride (h-BN) as nano-additives in military grade diesel engine oil. Materials Today: Proceedings, 50, 70-73.

19. Mishra, D., Mohapatra, S., &Satapathy, A. (2018). A detailed investigation on thermal and micro-structural properties of hexagonal boron nitride composites. Materials Today: Proceedings, 5(9), 19747-19753.

20. Chong, Y. M., Ye, Q., Yang, Y., Zhang, W. J., Bello, I., & Lee, S. T. (2010). Tribological study of boron nitride films. Diamond and related materials, 19(5-6), 654-660.

21. Charoo, M. S., &Wani, M. F. (2017). Tribological properties of h-BN nanoparticles as lubricant additive on cylinder liner and piston ring. Lubrication Science, 29(4), 241-254.

22. Kushwah, R., Jayan, M. S., Kanagasabapathy, H., Kumar, T. C. A., Halder, S., Begum, N., & Rajkumar, S. (2021). The impact of boron nitride (BN) on tribological behaviour of AZ84 magnesium matrix composites. Materials Today: Proceedings.

23. Jawaid, M., Nagarajan, R., Sukumaran, J., & De Baets, P. (Eds.). (2018). Synthesis and Tribological Applications of Hybrid Materials. John Wiley & Sons.

24. Asthana, R., Kumar, A. and Dahotre, N.B., 2006. Materials processing and manufacturing science. Elsevier

25. Bowden, F.P. and Leben, L., 1939. The nature of sliding and the analysis of friction. Proceedings of the Royal Society of London. Series A. Mathematical and Physical Sciences, 169(938), pp.371-391.

26. Chen, B., Bi, Q., Yang, J., Xia, Y. and Hao, J., 2008. Tribological properties of solid lubricants (graphite, h-BN) for Cu-based P/M friction composites. Tribology international, 41(12), pp.1145-1152.

27. Chen, J., Cheng, J., Li, F., Zhu, S., Qiao, Z. and Yang, J., 2016. The effect of compositional tailoring and sintering temperature on the mechanical and tribological properties of Cu/AlMgB14 composite. Tribology International, 96, pp.155-162.

28. Chen, X., Tao, J., Yi, J., Liu, Y., Li, C. and Bao, R., 2018. Strengthening behaviour of carbon nanotube-graphene hybrids in copper matrix composites. Materials Science and Engineering: A, 718, pp.427-436.

29. Chu, K., Wang, J., Liu, Y.P. and Gong, Z.R., 2018. Graphene defect engineering for optimizing the interface and mechanical properties of graphene/copper composites. Carbon, 140, pp.112-123.

30. Furlan, K.P., de Mello, J.D.B. and Klein, A.N., 2018. Self-lubricating composites containing MoS2: A review. Tribology International, 120, pp.280-298.

31. Gautam, R.K., Ray, S., Jain, S.C. and Sharma, S.C., 2008. Tribological behavior of Cu–Cr–SiCp in situ composite. Wear, 265(5-6), pp.902-912

32. Kumar, D.D., Kumar, N., Panda, K., Kirubaharan, A.K. and Kuppusami, P., 2018. Tribochemistry of contact interfaces of nanocrystalline molybdenum carbide films. Applied Surface Science, 447, pp.677-68

BIOGRAPHIES

1.Ganesh Chandra Lecturer in, Department of Mechanical Engineering, Sagar Institute Of Technology & Management Barabanki, Uttar Pradesh. India.